Supplementary Information (SI) for ChemComm.
This journal is © The Royal Society of Chemistry 2025

Supporting Information

Dual Regulation of Interface and Bulk Phase by a Multifunctional Additive for Constructing Stable Zinc-Sulfur Batteries

Xuewen Peng,[a] Caixiang Wang,[a] Qin Tang,[a] Yongjie Ye,[a] Ying Chen,[a] Mengqing Wang,[a] Xiaofei Jia,[a] Baojun Hou,[a] Hongbo Shu,[a] Xianyou Wang,[a] Ruizhi Yu,[*b] Tengfei Duan,[*c] Yongqian He,[*a] and Manfang Chen[*a]

a. National Base for International Science & Technology Cooperation of New Energy Equipment, Energy Storage Materials and Devices; National Local Joint Engineering Laboratory for Key Materials of New Energy Storage Battery; Hunan Province Key Laboratory of Electrochemical Energy Storage & Conversion; School of Chemistry, Xiangtan University, Xiangtan 411105, Hunan, China;

b. Institute of Micro/Nano Materials and Devices, Ningbo University of Technology, Ningbo, Zhejiang 315211, China;

c. School of Materials Science and Engineering, Hunan Key Laboratory of Electrochemical Green Metallurgy Technology, Hunan University of Technology, Zhuzhou 412007, PR China

Corresponding authors: Ruizhi Yu, E-mail: ruizhi.yu@nbut.edu.cn; Tengfei Du an, E-mail:duantf@hut.edu.cn; Yongqian He, E-mail: 202221531824@smail.xt u.edu.cn; Manfang Chen, E-mail: mfchen@xtu.edu.cn;

Experimental section

Electrolyte Preparation

The baseline electrolyte was synthesized through dissolution of 0.436 g zinc trifluoromethanesulfonate ($Zn(OTf)_2$) and 0.01596 g zinc iodide (ZnI_2) in 1 mL deionized water. Subsequently, the polyvinylpyrrolidone (PVP)-modified electrolyte was formulated by precisely weighing and dissolving 0.05 g of PVP into the baseline electrolyte.

Characterizations

The microscopic surface morphology of the Zn foil after the electrochemical reaction was characterized using field emission scanning electron microscopy (FESEM, JSM-7610 FPlus). Raman spectroscopy measurements were performed on an HR-800 spectrometer (HORIBA Jobin Yvon, France) equipped with a 632.8 nm laser source and a spot diameter of approximately 1 μm. All Raman spectra were calibrated against the characteristic peak of a single-crystal silicon wafer prior to the experiments to ensure data accuracy.

Electrochemical measurements

The cathode was fabricated by blending carbon materials (including self-synthesized NC materials), Ketjen Black (KB), and polyvinylidene fluoride (PVDF) in a mass ratio of 7:2:1 within N-methyl-2-pyrrolidone (NMP) solvent. After the evaporation of most NMP, the resulting slurry was coated onto a 10 mm carbon cloth and dried overnight at 60 °C. The prepared cathode sheets were then punched into circular discs, with the active material mass loading controlled at approximately 1.0 mg cm^{-2}. All electrochemical performance evaluations were conducted using a CR2032 coin-cell assembly system. During cell assembly, a glass fiber membrane (GF/D, Whatman) was employed as the separator. Galvanostatic charge-discharge tests were performed using a LAND-CT2001A battery test system. All assembled cells were allowed to rest for 12 hours prior to testing. For the Zn//Zn symmetric cells, two identical zinc foils (50 μm in thickness, 10 mm in diameter) were used as electrodes, separated by a glass fiber membrane (GF/D, Whatman). A volume of 150 μL of electrolyte was injected into each cell, which was then left to rest for 12 hours to ensure complete infiltration.

Computational details

All spin-polarized calculations were performed using the Vienna *ab initio* simulation package (VASP)[1-2] based on density generalized function theory (DFT). The electron exchange correlation was described by the gradient-corrected Perdew-Burke-Ernzerh (GGA-PBE) functional.[3] Ion-electron interaction was described by the projector augmented-wave (PAW) method.[4] We were built Zn (002) surfaces, and fix the bottom two layers of atoms during optimization. The cutoff energy was set to be 500 eV, and the total energy and force convergence for geometric optimization was set to 10^{-5} and 0.01 eV/Å, respectively. Integration in the Brilliouin zone was performed based on the Monkhorst-Pack scheme using a centered 3×3×1 k-point mesh in each primitive lattice

vector of the reciprocal space for optimization. The vacuum layer was set to 20 Å and a semi-empirical correction of DFT-D3[5] was adopted to account for the interaction of van der Waals forces. Charge density difference[6] analysis was performed to qualitatively describe the differences of charge distribution between adsorbate and substrate.

The adsorption energy ($\boldsymbol{E}_{ad}$) of various molecules (H_2O, PVP, I_3^-, HS^-) adsorbed onto the substrate can be written as

$$E_{ad} = E_{(sub\ +molecules)} - E_{(sub)} - E_{(molecules)}$$

S1

$E_{(sub\ +adsorbates)}$ is the total energy of various molecules adsorbed onto the substrate. $E_{(sub)}$ is the total energy of substrate. $E_{(molecules)}$ is the total energy of various molecules

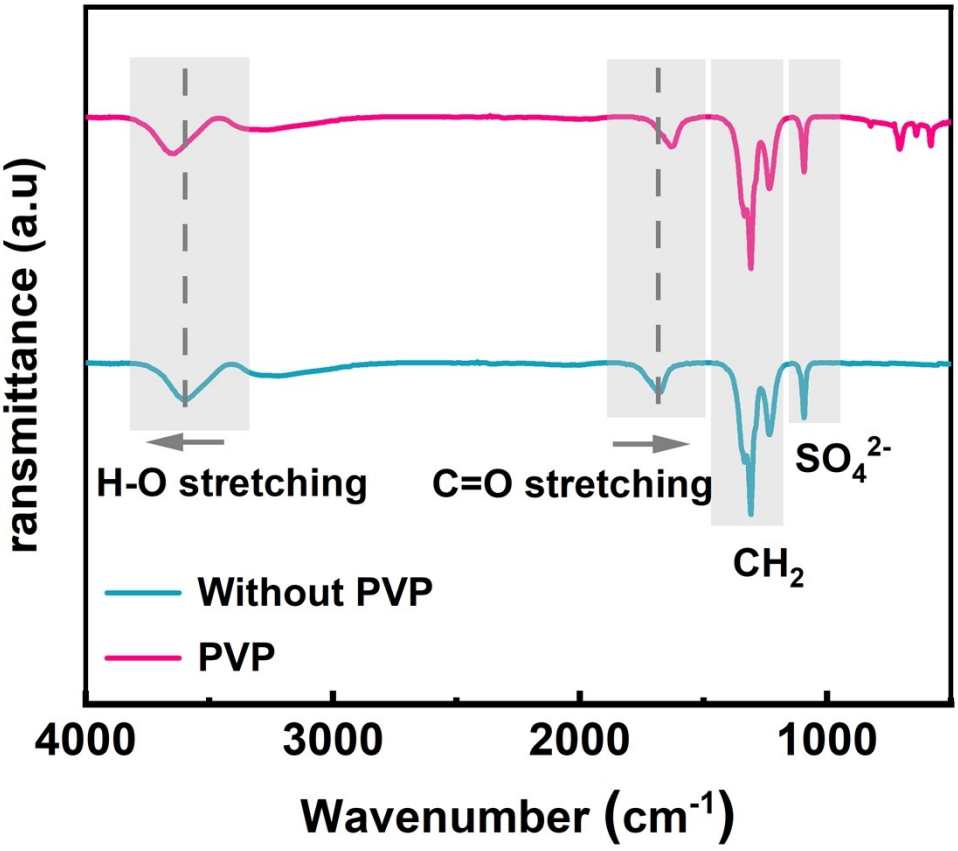

Fig. S1 Comparative FTIR spectra of the electrolytes with and without PVP additive.

Analysis of the infrared spectra reveals a distinct red-shift in the characteristic peak of the carbonyl group (C=O) in PVP, along with an overall shift toward higher wavenumbers in the O-H stretching vibration region of the FTIR spectrum. These two changes jointly demonstrate that an effective coordination interaction occurs between the carbonyl oxygen atoms in PVP and Zn^{2+} This interaction not only directly weakens the original hydrated sheath structure of Zn^{2+} but also significantly alters the hydrogen-bonding network of water molecules in the electrolyte[7].

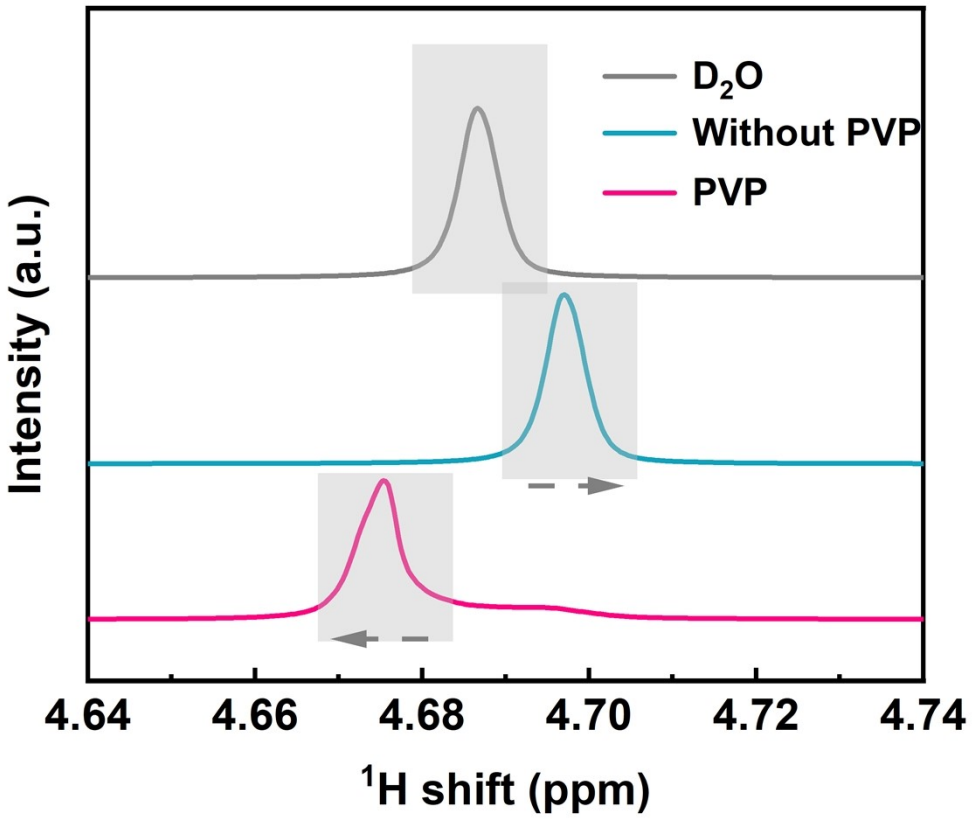

Fig. S2. 1H NMR spectra of the aqueous $Zn(OTf)_2$ electrolytes with and without PVP additive.

Analysis of the ^1H NMR spectra reveals that the upfield shift of the water proton peak directly confirms the alteration of the chemical environment of water molecules within the Zn^{2+} solvation sheath. This phenomenon indicates an increase in the electron cloud density of water molecules and an enhancement of the shielding effect, resulting from the coordination between PVP and Zn^{2+}. Such interaction weakens the interaction between water molecules and the central ion, thereby modifying their surrounding chemical microenvironment[8].

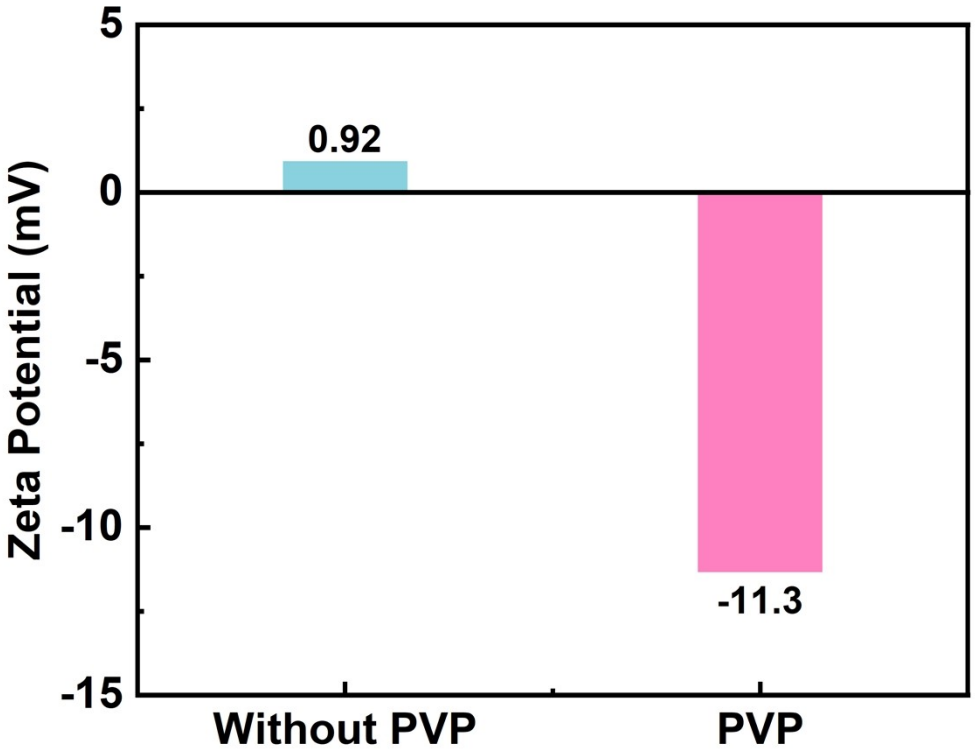

Fig. S3. Zeta potential of electrolytes with and without PVP additive.

Zeta potential measurements reveal that PVP addition markedly elevates the negative surface charge of colloidal particles. The resulting increased electrostatic repulsion at the interface not only enhances dispersion stability but also contributes to a more uniform ion transport.

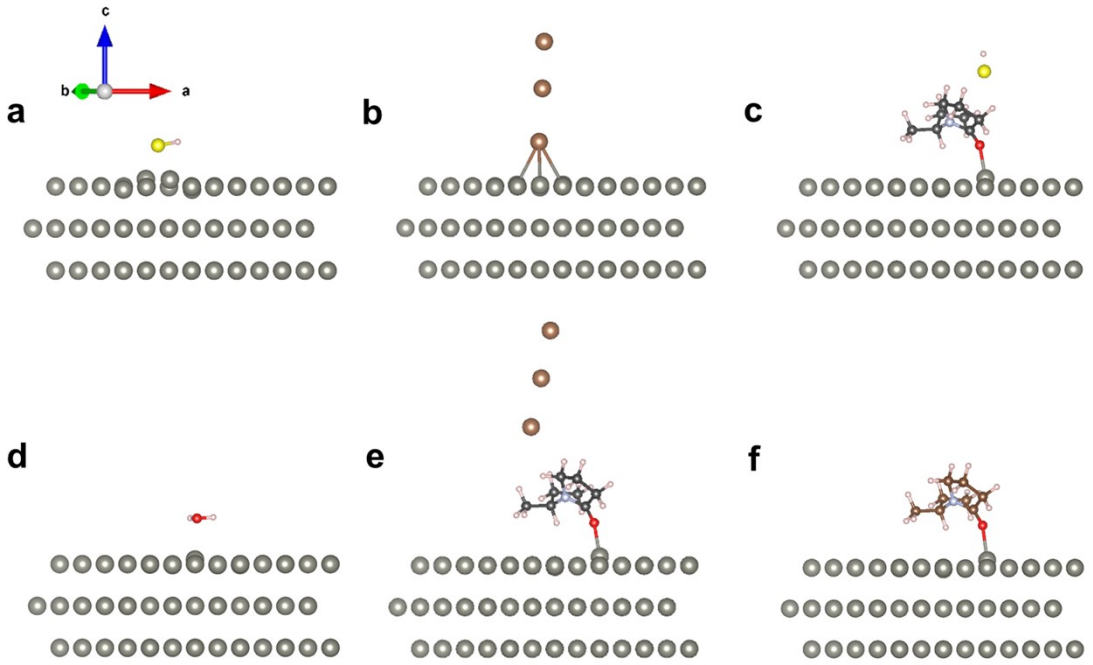

Fig. S4. Computational models of Zn (002) plane adsorption on (a) HS^-, (b) I_3^-, (c) with the co-adsorption of PVP and HS^-, (d) with the co-adsorption of PVP and I_3^-, (e) H_2O, and (f) PVP.

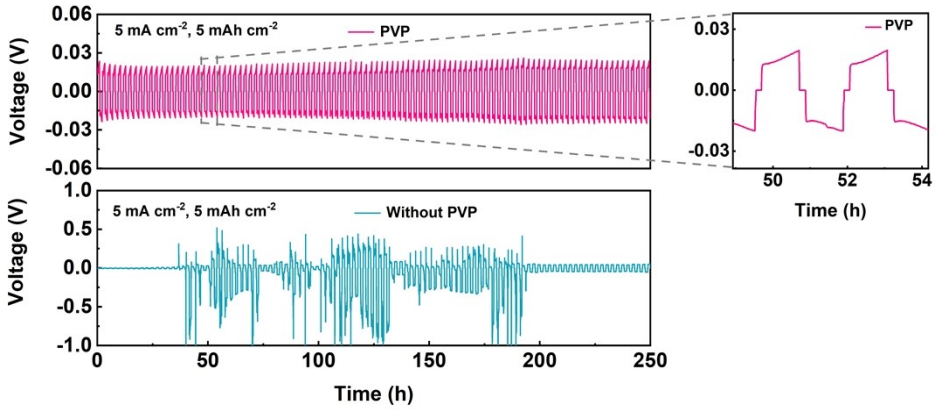

Fig. S5. Cycling performance of Zn||Zn symmetric cells. Voltage-time profiles at a current density of 5 mA cm^{-2} and an areal capacity of 5 mAh cm^{-2}.

Under testing conditions of 5 mA cm^{-2} and 5 mAh cm^{-2}, the results of Zn||Zn symmetric batteries show that the cell employing PVP-modified electrolyte maintains stable cycling for over 250 hours with a consistently steady polarization voltage, while the control cell using baseline electrolyte fails after only about 50 hours due to an internal short circuit caused by zinc dendrite growth.

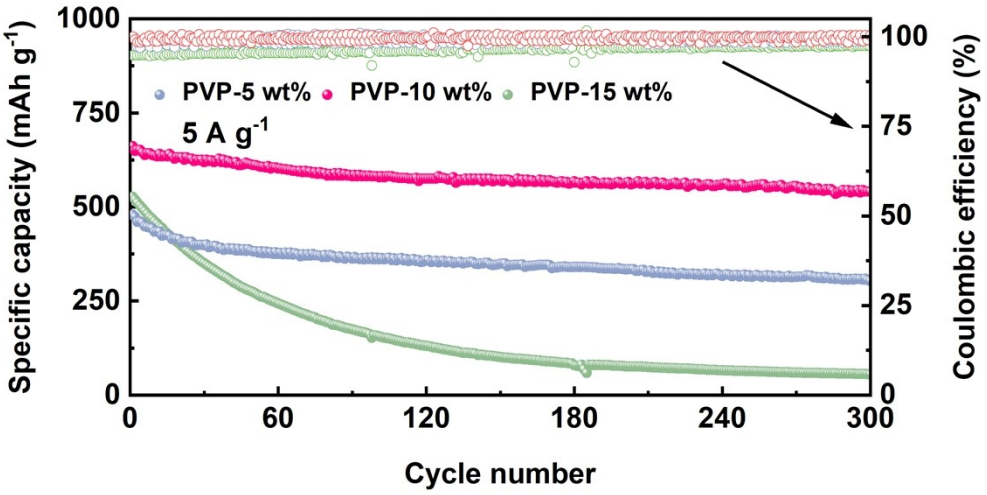

Fig. S6. Electrochemical performance comparison of Zn-S full cells with different PVP concentrations under long-term cycling at a current density of 5 A g^{-1}.

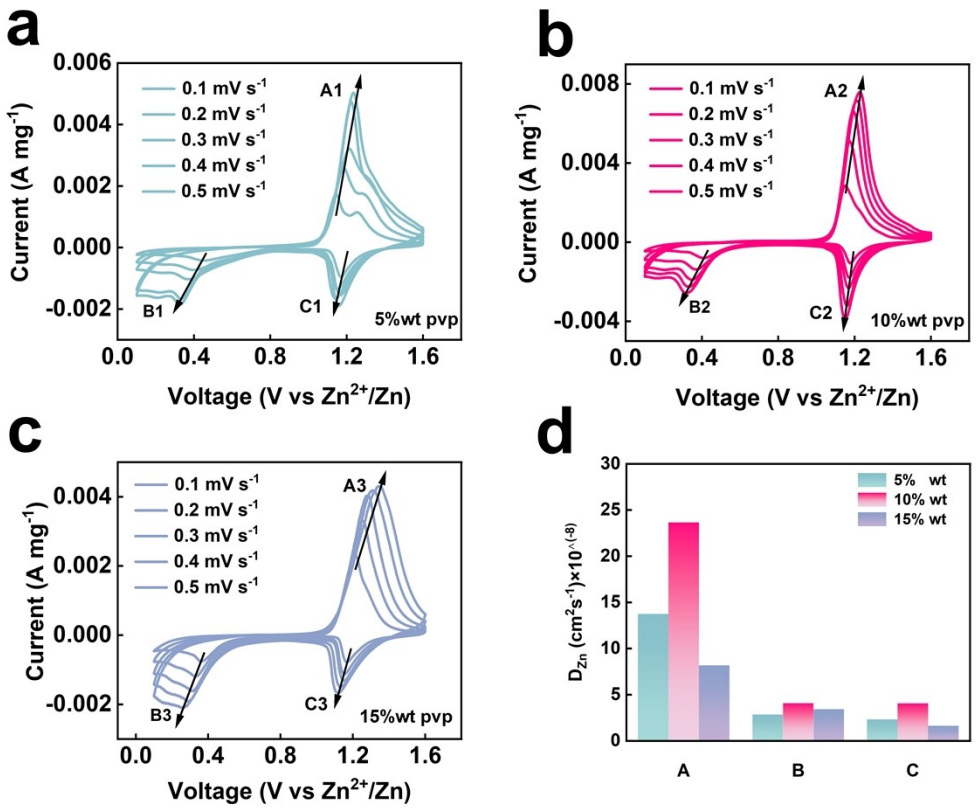

Fig. S7. (a-c) Cyclic voltammetry curves at various scan rates for cells containing electrolytes with (a) 5 wt%, (b) 10 wt%, and (c) 15 wt% PVP, respectively. (d) Comparison of the calculated apparent diffusion coefficients of Zn^{2+}.

Through systematic investigation of the effects of different PVP additive concentrations (5, 10, and 15 wt%) on the performance of zinc-sulfur batteries, 10 wt% was identified as the optimal concentration. Batteries with this concentration exhibited the highest cycling stability and coulombic efficiency. Scan-rate-dependent cyclic voltammetry analysis further revealed that the 10 wt% PVP system possessed the most reversible zinc deposition/dissolution behavior and the highest apparent diffusion coefficient of Zn^{2+}, confirming an optimal balance between interfacial kinetics and bulk transport. At an insufficient concentration (5 wt%), the CV curves showed larger polarization and lower peak currents, corresponding to inadequate interfacial protection that aggravated anode corrosion and dendrite growth. In contrast, an excessively high concentration (15 wt%) increased electrolyte viscosity, leading to weakened CV responses, decreased diffusion coefficients, and increased ion-migration resistance, thereby reducing battery capacity and rate performance.

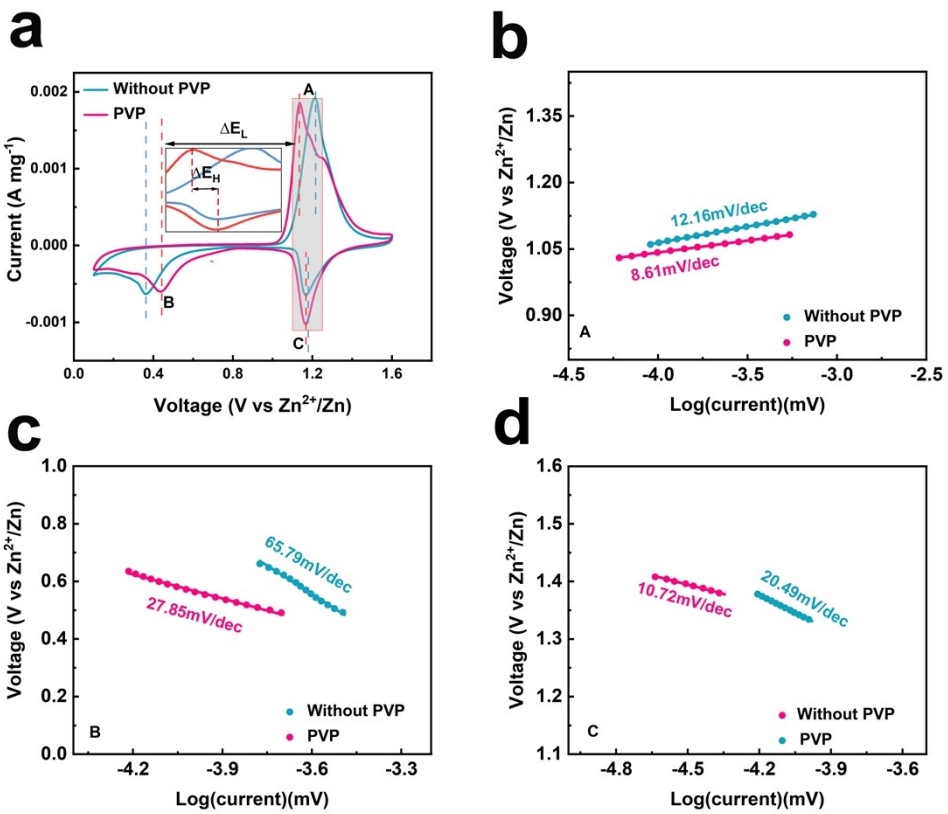

Fig. S8. (a) Comparison of CV curves at a scan rate of 0.1 mV s^{-1} (b-d) Tafel plots corresponding to peaks A, B, and C from the CV curves

Comparative analysis reveals that the introduction of PVP significantly enhances the current response in CV measurements (Figure a). Tafel analysis further confirms its kinetic optimization effect: during the high-voltage oxidation process (Figure b), PVP reduces the Tafel slope from 12.16 to 8.61 mV dec^{-1}, promoting the conversion of S_8 to soluble zinc polysulfides. In the low-voltage reduction processes (Figures c, d), the significantly lower Tafel slopes observed in the PVP-modified group demonstrate that the PVP additive effectively and synergistically enhances the redox reaction kinetics of zinc-sulfur batteries.

Fig. S9. Optical images of the Zn anode after cycling (left: with PVP-modified electrolyte, right: without PVP-modified electrolyte).

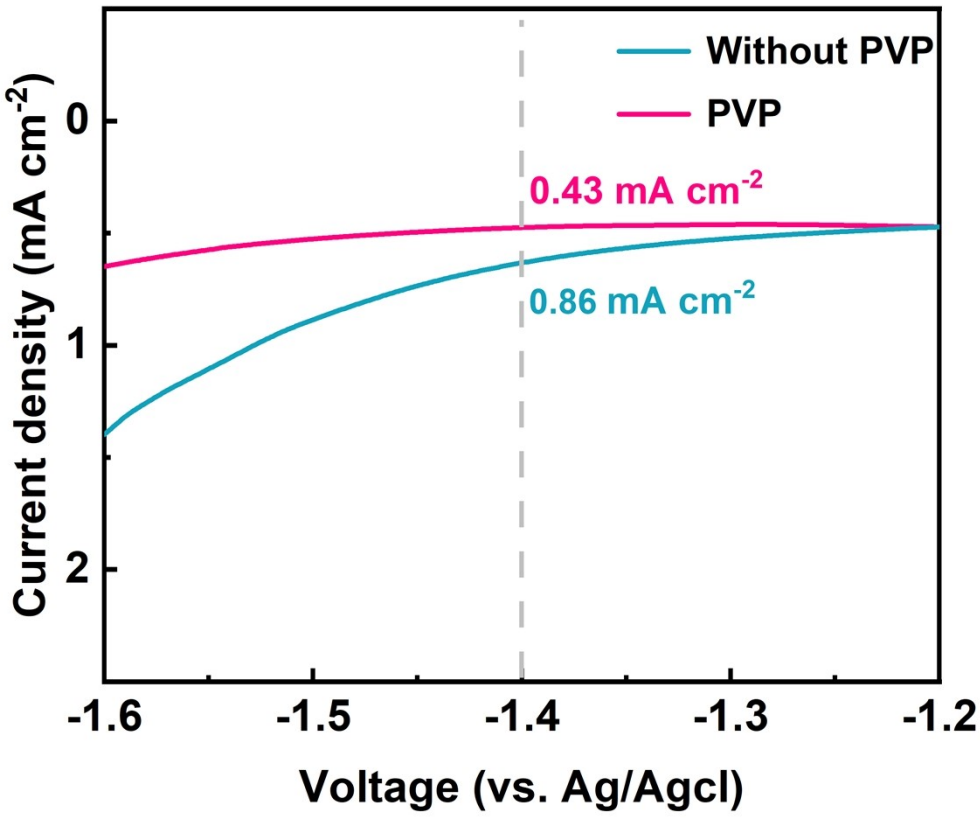

Fig. S10. Comparative LSV profiles evaluating the HER onset potential in different electrolytes.

Through LSV testing of the electrolyte, we further confirmed the excellent interfacial modulation capability of PVP. The results show that in the zinc deposition potential range, the cathodic current response of the electrolyte containing PVP is significantly suppressed. Especially within the key potential window of the HER, the current density of the PVP-containing system remains consistently at a very low level. This indicates that the passivation layer formed by PVP on the electrode surface effectively increases the overpotential of the hydrogen evolution reaction, thereby synergistically suppressing the HER side reaction from both thermodynamic and kinetic perspectives. This precise regulation of interfacial side reactions is the key reason why PVP-modified electrolytes can significantly enhance the reversibility and cycling stability of the zinc anode.

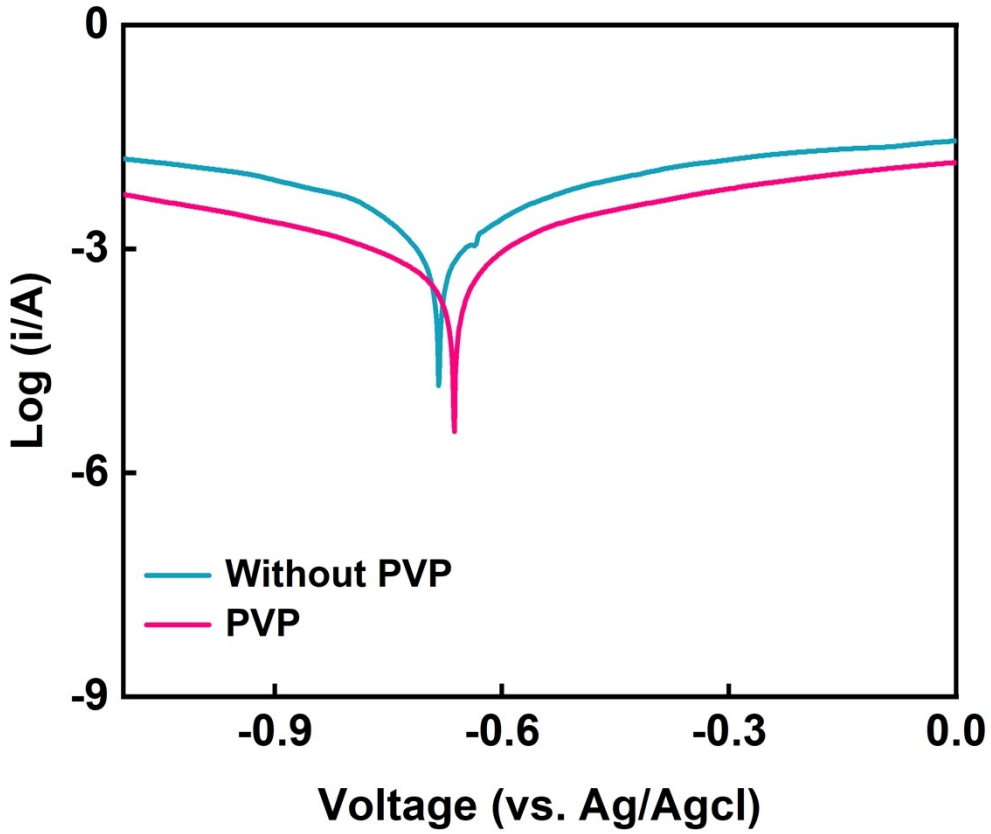

Fig. S11. Tafel polarization curves of zinc electrodes in different electrolytes

.

The Tafel test results indicate that after adding PVP, the corrosion current density of the zinc anode significantly decreased from -4.83 mA cm^{-2} to -5.45 mA cm^{-2}, while the corrosion potential shifted positively. These combined changes in kinetic parameters confirm that PVP effectively inhibits the hydrogen evolution corrosion reaction: the more positive corrosion potential indicates a reduced thermodynamic driving force for corrosion, and the lower corrosion current density further demonstrates a substantial decrease in the corrosion rate from a kinetic perspective

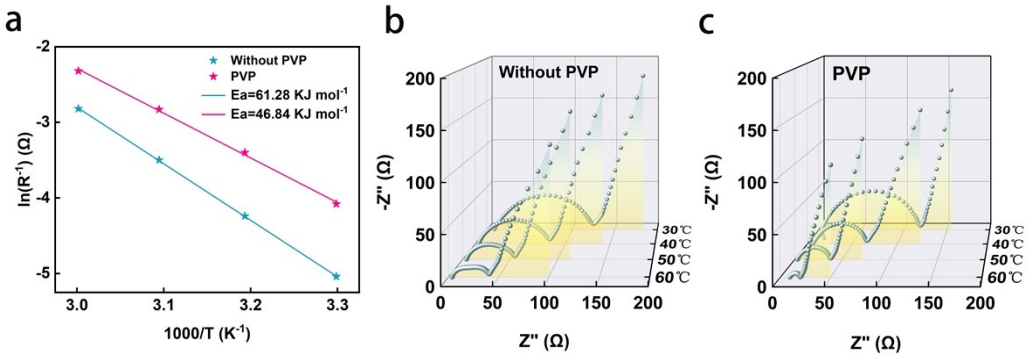

Figure S12. Activation energy for ion transport derived from variable-temperature conductivity measurements.

Based on the Arrhenius equation analysis, the activation energy for zinc deposition in the PVP-modified electrolyte is 46.84 kJ mol^{-1}, which is approximately 15% lower than that in the baseline electrolyte. This result demonstrates that PVP weakens the solvation sheath of Zn^{2+} through coordination between its carbonyl groups and Zn^{2+}, thereby reducing the energy required for the desolvation process. Simultaneously, the adsorption of PVP at the electrode interface optimizes the electrical double-layer structure, lowering the energy barrier for subsequent charge transfer. The improvement in this kinetic parameter corroborates the observed increase in Zn^{2+} transference number, decrease in corrosion current, and changes in solvation structure revealed by FTIR and ^{1}H NMR. These findings collectively demonstrate the dual-function mechanism of PVP.

Arrhenius equation:
$$ln\left(\frac{1}{R_{ct}}\right) = ln(A) - \frac{E_a}{R} \times \frac{1}{T} \quad \text{S2}$$

where Rct, A, Ea, R, and T are the charge-transfer resistance, Arrhenius constant, desolvated activation energy, gas constant, and absolute temperature, respectively[9].

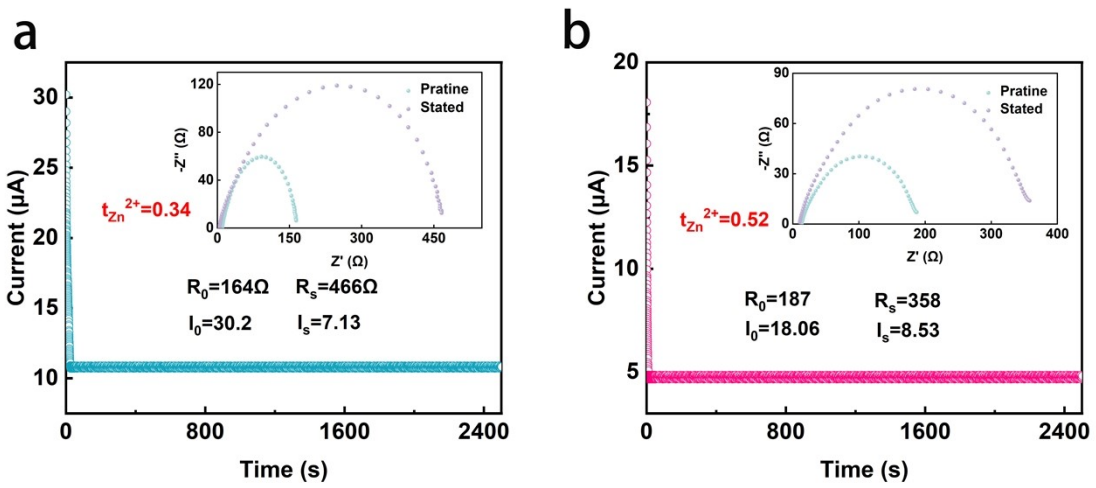

Figure S13. Determination of Zn2+ transference number via electrochemical impedance spectroscopy.

We determined the Zn^{2+} transport number using the Bruce–Vincent method. The results show that after adding PVP, t(Zn^{2+}) increased significantly from 0.34 in the baseline electrolyte to 0.52. This enhancement demonstrates that PVP promotes the directional migration of Zn2+ through its polymeric network while effectively restricting the migration of other competing ions such as H^+, thereby optimizing the ion transport selectivity in the bulk electrolyte, which helps alleviate concentration polarization at the electrode interface. This finding is further corroborated by the reduced activation energy for Zn^{2+} deposition, the decreased corrosion current density, and the observed changes in the Zn^{2+} solvation sheath structure from both FTIR and ^1H NMR spectroscopy-collectively confirming the dual functionality of PVP in modulating both the bulk electrolyte properties and the interfacial kinetics.

Transference number:

$$t^+ = \frac{I_s(\Delta V - I_0 R_0)}{I_0(\Delta V - I_s R_s)}$$

S3

where ΔV represents polarization potential of 10 mV, I_0 and I_s are the pristine and stated current, R_0 and R_s are R_{ct} measured by EIS[10].

	PVP	Without PVP
ΔV (mV)	10	10
R_0 (ohm)	187	164
R_s (ohm)	358	466
I_0 (μA)	18.06	30.2
I_s (μA)	8.53	7.13

t^+	0.52	0.34

References

[1] G. Kresse, J. Furthmüller, *Phys. Rev. B*. 1996, **54**, 11169, DOI: 10.1103/physrevb.54.11169.

[2] G. Kresse, J. Furthmüller, *Comput. Mater. Sci.* 1996, **6**, 15, DOI: 10.1016/0927-0256(96)00008-0.

[3] J. P. Perdew, K. Burke, M. Ernzerhof, *Phys. Rev. Lett*. 1996, **77**, 3865, DOI: 10.1103/physrevlett.77.3865.

[4] P. E. Blöchl, *Phys. Rev. B*. 1994, **50**, 17953, DOI: 10.1063/1.5078432.

[5] Grimme, S.; Antony, J.; Ehrlich, S.; Krieg, H. A Consistent and Accurate Ab Initio Parametrization of Density Functional Dispersion Correction (DFT-D) for the 94 Elements H-Pu. *J. Chem. Phys.* 2010, **132** (15), 154104, DOI: 10.1063/1.3382344.

[6] Wiberg, Kenneth B., et al. "Analysis of the effect of electron correlation on charge density distributions." *J. Phys. Chem.* (1992), **96**.2**:** 671-679, DOI: 10.1021/jp9527719.

[7] Q. B. Shen, T. Q. Chen, X. Li, S. X. Xia, T. Yuan, Y. P. Pang and S. Y. Zheng, *Sci. China Mater*, 2024, **67**, 2266-2276, DOI: 10.1007/s40843-023-2912-5.

[8] O. S. Ifayefunmi, P. J. Chimtali, A. O. Frimpong, Y. L. Wu, L. Y. Wen, Q. Zhou, M. Abdulhamid, Z. Mohamed, S. M. Chen, X. J. Wu, C. D. Wang and L. Song, *Adv. Sustainable Syst*, 2025, **9**, e01153, DOI: 10.1002/adsu.202501153.

[9] S. Z. Zhang, M. H. Ye, Y. F. Zhang, Y. C. Tang, X. Q. Liu and C. C. Li,

Adv. Funct. Mater, 2023, **33,** 2208230, DOI: 10.1002/adfm.202208230.

[10] M. Sun, G. C. Ji, M. Z. Li and J. P. Zheng, *Adv. Funct. Mater*, 2024, 34, 2402004, DOI: 10.1002/adfm.202402004.